nature materials

LETTERS

PUBLISHED ONLINE: 9 MAY 2010 | DOI: 10.1038/NMAT2753

# Dimensional crossover of thermal transport in few-layer graphene

Suchismita Ghosh[1], Wenzhong Bao[2], Denis L. Nika[1,3], Samia Subrina[1], Evghenii P. Pokatilov[1,3], Chun Ning Lau[2] and Alexander A. Balandin[1]*

**Graphene[1], in addition to its unique electronic[2,3] and optical properties[4], reveals unusually high thermal conductivity[5,6]. The fact that the thermal conductivity of large enough graphene sheets should be higher than that of basal planes of bulk graphite was predicted theoretically by Klemens[7]. However, the exact mechanisms behind the drastic alteration of a material's intrinsic ability to conduct heat as its dimensionality changes from two to three dimensions remain elusive. The recent availability of high-quality few-layer graphene (FLG) materials allowed us to study dimensional crossover experimentally. Here we show that the room-temperature thermal conductivity changes from ~2,800 to ~1,300 W m$^{-1}$ K$^{-1}$ as the number of atomic planes in FLG increases from 2 to 4. We explained the observed evolution from two dimensions to bulk by the cross-plane coupling of the low-energy phonons and changes in the phonon Umklapp scattering. The obtained results shed light on heat conduction in low-dimensional materials and may open up FLG applications in thermal management of nanoelectronics.**

One of the unresolved fundamental science problems[8], with enormous practical implications[9], is heat conduction in low-dimensional materials. The question of what happens with thermal conductivity when one goes to strictly two-dimensional (2D) and one-dimensional (1D) materials has attracted considerable attention[8,10–13]. Thermal transport in solids is described by thermal conductivity $K$ through the empirical Fourier law, which states that $\mathbf{J}_Q = -K\nabla T$, where the heat flux $\mathbf{J}_Q$ is the amount of heat transported through the unit surface per unit time and $T$ is temperature. This definition has been used for bulk materials as well as nanostructures. Many recent theoretical studies[8,10–13] suggest an emerging consensus that the intrinsic thermal conductivity of 2D and 1D anharmonic crystals is anomalous and reveals divergence with the size of the system defined either by the number of atoms $N$ or linear dimension $L$. In 2D this universal divergence leads to $K \sim \ln(N)$ (ref. 8). The anomalous nature of heat conduction in low-dimensional systems is sometimes termed as breakdown of Fourier's law[11]. The anomalous $K$ dependence on $L$ in strictly 2D (1D) materials should not be confused with the length dependence of $K$ in the ballistic transport regime frequently observed at low temperatures when $L$ is smaller than the phonon mean free path (MFP). Ballistic transport has been studied extensively in carbon nanotubes[14–16]. Here we focus on the diffusive transport and thermal conductivity limited by the intrinsic phonon interactions through Umklapp processes[17].

Experimental investigation of heat conduction in strictly 2D materials has essentially been absent owing to the lack of proper materials systems. Thermal transport in conventional thin films still retains 'bulk' features because the cross-sections of these structures are measured in many atomic layers. Heat conduction in such nanostructures is dominated by extrinsic effects, for example, phonon-boundary or phonon-defect scattering[18]. The situation has changed with the emergence of mechanically exfoliated graphene—an ultimate 2D system. It has been established experimentally that the thermal conductivity of large-area suspended single-layer graphene (SLG) is in the range $K \approx 3{,}000$–$5{,}000$ W m$^{-1}$K$^{-1}$ near room temperature[5,6], which is clearly above the bulk graphite limit $K \approx 2{,}000$ W m$^{-1}$K$^{-1}$ (ref. 7). The upper bound $K$ for graphene was obtained for the largest SLG flakes examined (~20 μm × 5 μm). The extraordinarily high value of $K$ for SLG is related to the logarithmic divergence of the 2D intrinsic thermal conductivity discussed above[7,8]. The MFP of the low-energy phonons in graphene and, correspondingly, their contribution to thermal conductivity are limited by the size of a graphene flake rather than by Umklapp scattering[7,19].

The dimensional crossover of thermal transport, that is, evolution of heat conduction as one goes from 2D graphene to 3D bulk, is of great interest for both fundamental science[8] and practical applications[9]. We addressed this problem experimentally by measuring the thermal conductivity of FLG as the number of atomic planes changes from $n = 2$ to $n \approx 10$. A high-quality large-area FLG sheet, where the thermal transport is diffusive and limited by intrinsic rather than extrinsic effects, is an ideal system for such a study. A number of FLG samples were prepared by standard mechanical exfoliation of bulk graphite[1] and suspended across trenches in $Si/SiO_2$ wafers (Fig. 1a–c). The depth of the trenches was ~300 nm and the trench width varied in the range 1–5 μm. Metal heat sinks near the trench edges were fabricated by shadow mask evaporation. We used our previous experience in graphene device fabrication[20] to obtain the highest quality set of suspended samples. The width of the suspended flakes varied from $W \approx 5$ to 16 μm. The number of atomic layers in the graphene flakes was determined with micro-Raman spectroscopy (InVia, Renishaw) through deconvolution of the 2D/G′ band in graphene's spectrum[21]. The measurements of $K$ were carried out using a steady-state optical technique developed by us on the basis of micro-Raman spectroscopy[5]. The shift of the temperature-sensitive Raman G peak in graphene's spectrum[22] defined the local temperature rise in the suspended portion of FLG in response to heating by an excitation laser in the middle of the suspended portion of the flakes (Fig. 1d). The thermal conductivity was extracted from the power dissipated in FLG, the resulting temperature rise and the flake geometry through the finite-element method solution of the heat diffusion equation (Fig. 1e; see the Methods section).

[1]Nano-Device Laboratory, Department of Electrical Engineering and Materials Science and Engineering Program, University of California–Riverside, Riverside, California 92521, USA, [2]Department of Physics and Astronomy, University of California–Riverside, Riverside, California 92521, USA, [3]Department of Theoretical Physics, State University of Moldova, Chisinau MD-2009, Republic of Moldova. *e-mail: balandin@ee.ucr.edu.

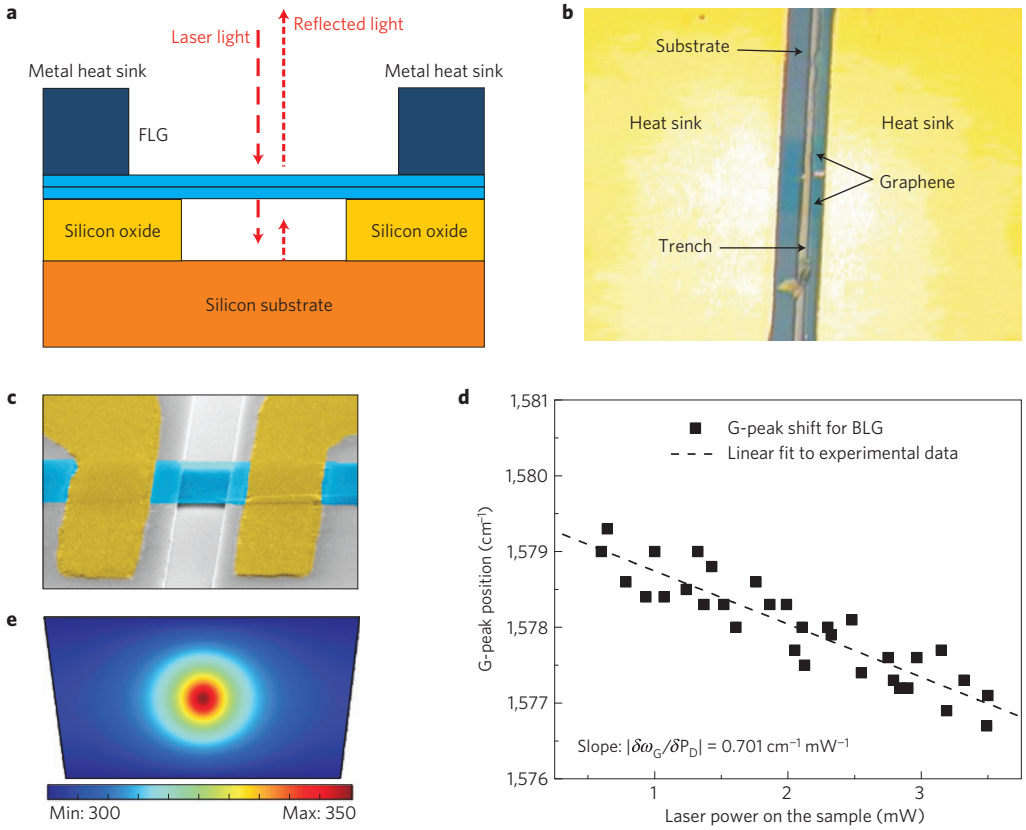


**Figure 1 | Samples and measurement procedure. a**, Schematic of the thermal conductivity measurement showing suspended FLG flakes and excitation laser light. **b**, Optical microscopy images of FLG attached to metal heat sinks. **c**, Coloured scanning electron microscopy image of the suspended graphene flake to clarify a typical structure geometry. **d**, Experimental data for Raman G-peak position as a function of laser power, which determines the local temperature rise in response to the dissipated power. **e**, Finite-element simulation of temperature distribution in the flake with the given geometry used to extract the thermal conductivity.

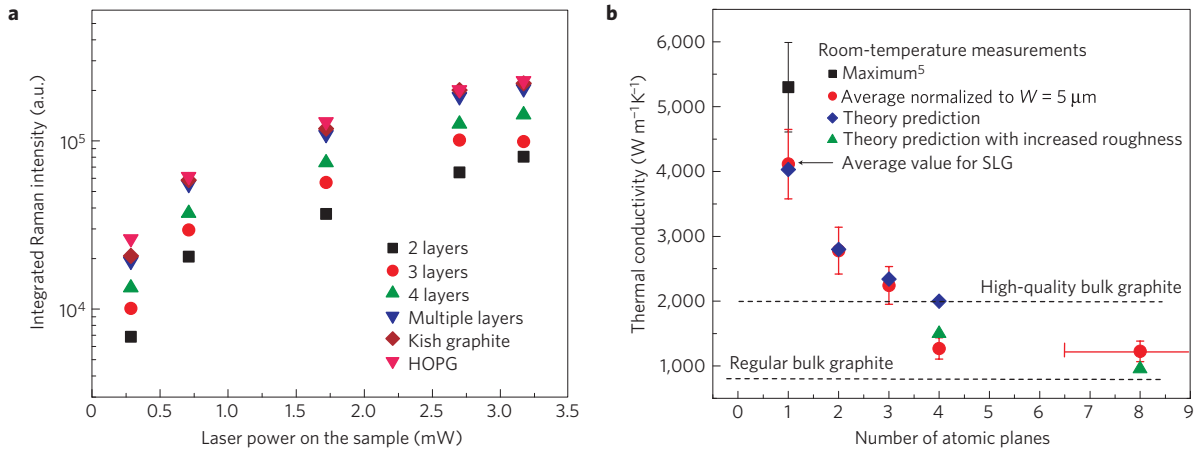


**Figure 2 | Experimental data. a**, Integrated Raman intensity of the G peak as a function of the laser power at the sample surface for FLG and reference bulk graphite (Kish and highly ordered pyrolytic graphite (HOPG)). The data were used to determine the fraction of power absorbed by the flakes. **b**, Measured thermal conductivity as a function of the number of atomic planes in FLG. The dashed straight lines indicate the range of bulk graphite thermal conductivities. The blue diamonds were obtained from the first-principles theory of thermal conduction in FLG based on the actual phonon dispersion and accounting for all allowed three-phonon Umklapp scattering channels. The green triangles are Callaway–Klemens model calculations, which include extrinsic effects characteristic for thicker films.

The power dissipated in FLG was determined through the calibration procedure based on comparison of the integrated Raman intensity of FLG's G peak $I^{G}_{FLG}$ and that of reference bulk graphite $I^{G}_{BULK}$. Figure 2a shows measured data for FLG with $n = 2$, 3, 4, ~8 and reference graphite. Each addition of an atomic plane leads to an $I^{G}_{FLG}$ increase and convergence with the graphite whereas the ratio $\varsigma = \overline{I^{G}_{FLG}}/\overline{I^{G}_{BULK}}$ stays roughly independent of excitation power, indicating proper calibration. In Fig. 2b we present measured $K$ as a function of the number of atomic planes $n$ in FLG. The maximum and average $K$ values for SLG are also shown. As graphene's $K$ depends on the width of the flakes[19,23] the data for FLG are normalized to the width $W = 5\,\mu m$ to

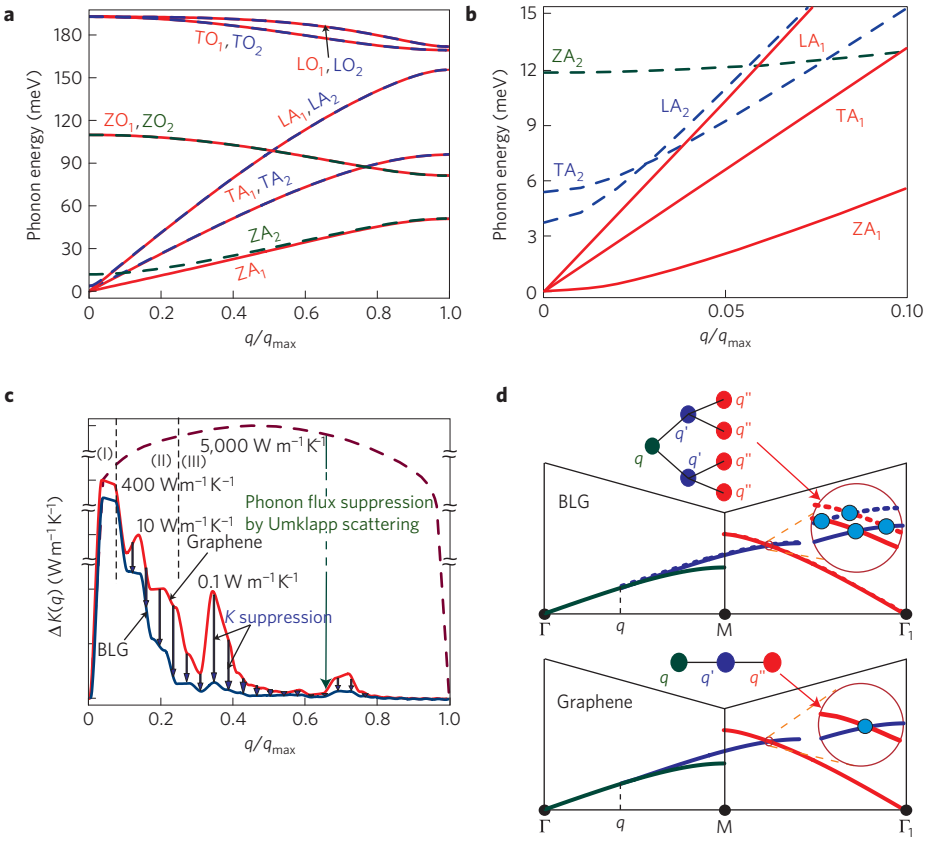


**Figure 3 | Theoretical interpretation. a**, Phonon dispersion in BLG, which shows that phonon branches are double degenerate for $q > 0.2q_{max}$ (where $q_{max} = 14.749\,nm^{-1}$). **b**, Close-up of the phonon dispersion in graphene (solid curves) and BLG (solid and dashed curves) near the Brillouin zone centre. Note that the longitudinal acoustic ($LA_2$) and transverse acoustic ($TA_2$) phonon branches in BLG have a very small slope at low $q$, which translates to a low phonon group velocity. **c**, Contributions to thermal conductivity of different phonons, indicating the range of phonon wavevectors where Umklapp scattering is the main thermal-transport-limiting mechanism. The dashed line corresponds to the rough-edge scattering alone. **d**, Diagram of three-phonon Umklapp scattering in graphene and BLG, which shows that in BLG there are more states available for scattering owing to the increased number of phonon branches.

allow for direct comparison. At fixed $W$ the changes in the $K$ value with $n$ mostly result from modification of the three-phonon Umklapp scattering. The thermal transport in our experiment is in the diffusive regime because $L$ is larger than the phonon MFP in graphene, which was measured[6] and calculated[24] to be around ~800 nm near room temperature. Thus, we explicitly observed heat conduction crossover from 2D graphene to 3D graphite as $n$ changes from 2 to ~8.

It is illustrative that the measured $K$ dependence on FLG thickness $h \times n$ ($h = 0.35$ nm) is opposite from what is observed for conventional thin films with thicknesses in the range of a few nanometres to micrometres. In conventional films with thickness $H$ smaller than the phonon MFP, thermal transport is dominated by phonon-rough-boundary scattering. The thermal conductivity can be estimated from $K = (1/3)C_V v^2 \tau$, where $C_V$ is the specific heat and $v$ and $\tau$ are the average phonon velocity and lifetime. When the phonon lifetime is limited by the boundary scattering, $\tau = \tau_B$, one can use the Ziman formula, $(1/\tau_B) = (v/H)((1-p)/(1+p))$, which shows that $K$ scales down with decreasing thickness (here $p$ is a parameter defined by the surface roughness). In FLG with 2 or 3 atomic layer thickness there is essentially no scattering from the top and back surfaces (only the edge scattering is present[23]). Indeed, FLG is too thin for any cross-plane velocity component and for random thickness fluctuations, that is, $p \approx 1$ for FLG. To understand the thermal crossover one needs to examine the changes in the intrinsic scattering mechanisms limiting $K$: Umklapp scattering resulting from crystal anharmonicity.

The crystal structure of bilayer graphene (BLG) consists of two atomic planes of graphene bound by weak van der Waals forces resulting in a phonon dispersion different from that in SLG (Fig. 3a,b). By calculating the phonon dispersion in FLG from first principles[23,25], we were able to study phonon dynamics (Supplementary Movie) and the role of separate phonon modes. Figure 3c shows the contributions $\Delta K(q_i)$ to the thermal conductivity of phonons with wavevectors from the interval $(q_i, q_{i+1})$. These contributions, counted over the whole Brillouin zone, make up the total $K = \int_0^{q_{max}} K(q)\,dq = \sum_1^m \Delta K(q_i)$, which is, in our calculation, limited by the phonon Umklapp and edge boundary scattering ($m$ is the number of intervals $(q_i, q_{i+1})$ and $p = 0.92$ for the edges). In BLG the number of available phonon branches doubles (Fig. 3a,b). However, the new conduction channels do not transmit heat effectively in the low-energy regime because the group velocities of the $LA_2$ and $TA_2$ branches are close to zero at small $q$. On the other hand, an increase in the thickness $h \times n$ leads to a corresponding decrease in the flux density: see region I of small $q$ where thermal transport is mostly limited by edge scattering (Fig. 3c). In region III of large $q$, the number of phonon states available for three-phonon Umklapp scattering in BLG increases by a factor of four as compared with SLG (Fig. 3d). As a result, despite the increase in the number of conduction channels in BLG, its $K$ decreases because the $q$ phase space available for Umklapp scattering increases even more (Supplementary Materials). One can say that in SLG, phonon Umklapp scattering is quenched and the heat transport is limited mostly by the edge (in-plane) boundary

scattering. This is in agreement with Klemens's explanation of the higher thermal conductivity of graphene compared with graphite[7]. It is rooted in the fundamental properties of 2D systems discussed above. Our theory also explains molecular-dynamics simulations for 'unrolled' carbon nanotubes, which revealed a much higher $K$ for graphene than for graphite[26]. The theoretical data points for $n = 1$–4 shown in Fig. 2b are in excellent agreement with the experiment. They were obtained by accounting for all allowed Umklapp processes through extension of the diagram technique developed by us for SLG (ref. 23) to $n = 2$ and 3. The lower measured $K$ values for $n = 4$ are explained by the stronger extrinsic effects resulting from difficulties in maintaining the thickness uniformity in such samples. The theoretical data point approaches the bulk limit for the 'ideal' graphite. It is possible that the crossover point may be related to AB Bernal stacking and completeness of the graphite unit cell. Practically, its position is affected by many factors including FLG's quality, the width of the flake and the strength of substrate coupling.

Thus, we have experimentally demonstrated 2D → 3D-dimensional crossover of heat conduction in FLG. We related the increased thermal conductivity of graphene to the fundamental properties of 2D systems and determined the physical mechanisms behind the thermal conductivity reduction in few-atom-thick crystals. The obtained results are important for the proposed graphene and FLG applications in nanoelectronics.

## Methods

The trenches in the $Si/SiO_2$ wafers were made using reactive ion etching (STS). The evaporated metal heat sinks ensured proper thermal contact with the flakes and a constant temperature during the measurements (Fig. 1b,c). FLG samples were heated with a 488 nm laser (argon ion) in the middle of the suspended part (Fig. 1a). The size of the laser spot was determined to be 0.5–1 μm. The diameter of the heated region on the flake was larger owing to the indirect nature of energy transfer from light to phonons. The laser light deposits its energy to electrons, which propagate with Fermi velocity $v_F \approx 10^6$ m s$^{-1}$. The characteristic time for energy transfer from electrons to phonons is of the order of $\tau_{ph} \sim 10^{-12}$ s (refs 27,28). The measurement time in our steady-state technique is a few minutes, which is much larger than $\tau_{ph}$ but at the same time, much smaller than the time required to introduce any laser-induced damage to the sample. The correction to the hot-spot size is estimated as $l_{e-ph} = v_F \tau_{ph} \sim 1$ μm. Strain, stress and surface charges change the G-peak position in Raman spectra and may lead to its splitting[29,30]. Strain and doping may also affect the thermal conductivity. To minimize these effects, we selected samples where a symmetric and narrow G peak was in its 'standard' location (∼1,579 cm$^{-1}$) characteristic for the undoped unstrained graphene[21,22,29,30]. No bias was applied to avoid charge accumulation[30]. It was not possible to mechanically exfoliate FLG flakes with different numbers of atomic planes $n$ and the same geometry. To avoid damage to the graphene, the obtained flakes were not cut to the same shape. Instead, we solved the heat diffusion equation numerically for each sample shape to extract its thermal conductivity (Fig. 1e). This was accomplished through an iteration procedure (Supplementary Information) for the Gaussian-distributed laser intensity and an effective spot size corrected to account for $l_{e-ph}$. The errors associated with the laser spot size and intensity variation were ∼8%, that is, smaller than the error associated with the local temperature measurement by Raman spectrometers (∼10–13%) determined by the spectral resolution of the instrument and random experimental data spread (see Fig. 2b). The effects of the thermal contact resistance were eliminated by using large-sized metallic heat sinks and ensuring a large FLG–sink contact area.

Received 22 October 2009; accepted 24 March 2010; published online 9 May 2010

## References


1. Novoselov, K. S. *et al.* Electric field effect in atomically thin carbon films. *Science* **306,** 666–669 (2004).
2. Novoselov, K. S. *et al.* Two-dimensional gas of massless Dirac fermions in graphene. *Nature* **438,** 197–200 (2005).
3. Zhang, Y. B., Tan, Y. W., Stormer, H. L. & Kim, P. Experimental observation of the quantum Hall effect and Berry's phase in graphene. *Nature* **438,** 201–204 (2005).
4. Nair, R. R. *et al.* Fine structure constant defines visual transparency of graphene. *Science* **320,** 1308 (2008).
5. Balandin, A. A. *et al.* Superior thermal conductivity of single-layer graphene. *Nano Lett.* **8,** 902–907 (2008).
6. Ghosh, S. *et al.* Extremely high thermal conductivity of graphene: Prospects for thermal management applications in nanoelectronic circuits. *Appl. Phys. Lett.* **92,** 151911 (2008).
7. Klemens, P. G. Theory of the a-plane thermal conductivity of graphite. *J. Wide Bandgap Mater.* **7,** 332–339 (2000).
8. Lepri, S., Livi, R. & Politi, A. Thermal conduction in classical low-dimensional lattices. *Phys. Rep.* **377,** 1–80 (2003).
9. Balandin, A. A. Chill out: New materials and designs can keep chips cool. *IEEE Spectr.* 35–39 (2009).
10. Narayan, O. & Ramaswamy, S. Anomalous heat conduction in one-dimensional momentum-conserving systems. *Phys. Rev. Lett.* **89,** 200601 (2002).
11. Chang, C. W., Okawa, D., Garcia, H., Majumdar, A. & Zettl, A. Breakdown of Fourier's law in nanotube thermal conductors. *Phys. Rev. Lett.* **101,** 075903 (2008).
12. Basile, G., Bernardin, C. & Olla, S. Momentum conserving model with anomalous thermal conductivity in low dimensional systems. *Phys. Rev. Lett.* **96,** 204303 (2006).
13. Yang, L., Grassberger, P. & Hu, B. Dimensional crossover of heat conduction in low dimensions. *Phys. Rev. E* **74,** 062101 (2006).
14. Che, J., Çağin, T. & Goddard, W. A. III Thermal conductivity of carbon nanotubes. *Nanotechnology* **11,** 65–69 (2000).
15. Mingo, N. & Broido, D. A. Carbon nanotube ballistic thermal conductance and its limits. *Phys. Rev. Lett.* **95,** 096105 (2005).
16. Kim, P., Shi, L., Majumdar, A. & McEuen, P. L. Thermal transport measurements of individual multiwalled nanotubes. *Phys. Rev. Lett.* **87,** 215502 (2001).
17. Srivastava, G. P. *The Physics of Phonons* (IOP Publishing Ltd, 1990).
18. Hochbaum, A. I. *et al.* Enhanced thermoelectric performance of rough silicon nanowires. *Nature* **451,** 163–167 (2008).
19. Nika, D. L., Ghosh, S., Pokatilov, E. P. & Balandin, A. A. Lattice thermal conductivity of graphene flakes: Comparison with bulk graphite. *Appl. Phys. Lett.* **94,** 203103 (2009).
20. Bao, W. Z. *et al.* Controlled ripple texturing of suspended graphene and ultrathin graphene membranes. *Nature Nanotech.* **4,** 562–566 (2009).
21. Ferrari, A. C. *et al.* Raman spectrum of graphene and graphene layers. *Phys. Rev. Lett.* **97,** 187401 (2006).
22. Calizo, I., Balandin, A. A., Bao, W., Miao, F. & Lau, C. N. Temperature dependence of the Raman spectra of graphene and graphene multi-layers. *Nano Lett.* **7,** 2645–2649 (2007).
23. Nika, D. L., Pokatilov, E. P., Askerov, A. S. & Balandin, A. A. Phonon thermal conduction in graphene: Role of Umklapp and edge roughness scattering. *Phys. Rev. B* **79,** 155413 (2009).
24. Hu, J., Ruan, X. & Chen, Y. P. Thermal conductivity and thermal rectification in graphene nanoribbons: A molecular dynamics study. *Nano Lett.* **9,** 2730–2735 (2009).
25. Mounet, N. & Marzari, N. First-principles determination of the structural, vibrational and thermodynamic properties of diamond, graphite, and derivatives. *Phys. Rev. B* **71,** 205214 (2005).
26. Berber, S., Kwon, Y-K. & Tomanek, D. Unusually high thermal conductivity of carbon nanotubes. *Phys. Rev. Lett.* **84,** 4613–4616 (2000).
27. Dawlaty, J. M., Shivaraman, S., Chandrashekhar, M., Rana, F. & Spencer, M. G. Measurement of ultrafast carrier dynamics in epitaxial graphene. *Appl. Phys. Lett.* **92,** 042116 (2008).
28. Bistritzer, R. & MacDonald, A. H. Electronic cooling in graphene. *Phys. Rev. Lett.* **102,** 206410 (2009).
29. Mohiuddin, T. M. G. *et al.* Uniaxial strain in graphene by Raman spectroscopy: G peak splitting, Grüneisen parameters, and sample orientation. *Phys. Rev. B* **79,** 205433 (2009).
30. Berciaud, S., Ryu, S., Brus, L. E. & Heinz, T. F. Probing the intrinsic properties of exfoliated graphene: Raman spectroscopy of free-standing monolayers. *Nano Lett.* **9,** 346–352 (2009).


## Acknowledgements

A.A.B. acknowledges support from ONR through award N00014-10-1-0224, ARL/AFOSR through award FA9550-08-1-0100 and SRC - DARPA through the FCRP Center on Functional Engineered Nano Architectonics (FENA) and the Interconnect Focus Center (IFC). C.N.L. and W.B. acknowledge support from ONR/DMEA H94003-09-2-0901, NSF/CBET 0854554 and GRC.

## Author contributions

A.A.B. conceived the experiment, led the data analysis, proposed theoretical interpretation and wrote the manuscript; S.G. carried out Raman measurements; S.S. carried out finite-element modelling for thermal data extraction; W.B. prepared most of the samples; C.N.L. supervised the sample fabrication; D.L.N. and E.P.P. assisted with theory development and carried out computer simulations of thermal conductivity.

## Additional information

The authors declare no competing financial interests. Supplementary information accompanies this paper on www.nature.com/naturematerials. Reprints and permissions information is available online at http://npg.nature.com/reprintsandpermissions. Correspondence and requests for materials should be addressed to A.A.B.